Towards relativistic orbit fitting of Galactic center stars and pulsars

Raymond Angélil and Prasenjit Saha

Institute for Theoretical Physics, University of Zürich,
Winterthurerstrasse 190, CH-8057 Zürich, Switzerland

and

David Merritt

Department of Physics and Center for Computational Relativity and Gravitation,
Rochester Institute of Technology,
Rochester, NY 14623

ABSTRACT

The S stars orbiting the Galactic center black hole reach speeds of up to a few percent the speed of light during pericenter passage. This makes, for example, S2 at pericenter much more relativistic than known binary pulsars, and opens up new possibilities for testing general relativity. This paper develops a technique for fitting nearly-Keplerian orbits with perturbations from Schwarzschild curvature, frame dragging, and spin-induced torque, to redshift measurements distributed along the orbit but concentrated around pericenter. Both orbital and light-path effects are taken into account. It turns out that absolute calibration of rest-frame frequency is not required. Hence, if pulsars on orbits similar to the S stars are discovered, the technique described here can be applied without change, allowing the much greater accuracies of pulsar timing to be taken advantage of. For example, pulse timing of $3\,\mu s$ over one hour amounts to an effective redshift precision of $30\,\mathrm{cm\,s^{-1}}$, enough to measure frame dragging and the quadrupole moment from an S2-like orbit, provided problems like the Newtonian "foreground" due to other masses can be overcome. On the other hand, if stars with orbital periods of order a month are discovered, the same could be accomplished with stellar spectroscopy from the E-ELT at the level of $1\,\mathrm{km\,s^{-1}}$.

1. Introduction

Tracing the orbits of the S stars in the Galactic center region reveals a central mass of $\sim 4 \times 10^6 M_\odot$ (Ghez et al. 2008; Gillessen et al. 2009a), presumably a supermassive black hole. The roughly 20 known S stars are mostly main-sequence B stars, and it is likely that they share their environment with many fainter stars. Hence discovery by the next generation of telescopes of stars far closer to the black hole is anticipated. The dynamics of the orbit and light trajectories provide an opportunity to test hitherto unobserved predictions of general relativity in the black hole neighborhood, and in doing so, confirm or revise our understanding of the nature of gravity (Gillessen et al. 2010). Meanwhile, searches for pulsars in the Galactic-center region are also underway (e.g., Macquart et al. 2010). If pulsars on orbits similar to S stars are discovered, their time-of-arrival measurements may provide accuracies orders of magnitude beyond those available from optical spectroscopy.

It is interesting to compare S stars with other relativistic orbits. General relativistic perturbations of a nearly Keplerian orbit typically scale as an inverse power of the classical angular momentum $\sqrt{a(1-e^2)}$. So a simple measure of the strength of

relativistic effects in a nearly Keplerian orbit is the dimensionless pericenter distance.[*] Figure 1 plots pericenter distance against orbital period for a sample of S stars and binary pulsars, together with Mercury and artificial satellites. At present, binary pulsars are the leading laboratories for general relativity. The principles are summarized in Taylor (1994). Taylor's Figure 11, depicting five intersecting curves, indicating four distinct tests of general relativity, is especially memorable, and descendants of this figure with newer data appear in recent work (e.g., Figure 3 in Kramer & Wex 2009). So it is remarkable that the star S2 has a pericenter distance $\sim 3 \times 10^3$, an order of magnitude lower than the most relativistic binary-pulsar systems, and four orders of magnitude lower than Mercury. This suggests that Galactic center orbits may show relativistic effects not measured in binary pulsars, such as frame dragging. On the other hand, S2 has an orbital period of $\sim 15.9\,\mathrm{yr}$ versus one day or less for some binary pulsars. Thus, for the known S stars, or pulsars on similar orbits, we cannot build up a relativistic signal over many orbits. A different strategy is needed, based on detailed observation of one or a few orbits, and paying special attention to pericenter passage, when relativistic effects are strongest.

Several different possibilities for observing relativistic effects have been discussed in the literature. To see how these relate to each other, let us consider the different physical effects involved in observing a relativistic orbit over time. These are illustrated in Figure 2. Shown schematically in this figure is a star on a precessing orbit, which emits photons (pulses, wavecrests) at a fixed frequency in proper time. These photons then take a curved path to the observer. When they arrive, both their frequency and their travel direction have been altered. What can the observer detecting these photons infer about the metric? This observer must take multiple physical processes into account.

1. *Time dilation* at the source is a consequence of the equivalence principle, and is the strongest relativistic perturbation. Its measurability in the context of the Global Positioning System (GPS) is well known (Ashby 2003). The manifestation of time dilation in pulsar timing is known as the Einstein time delay. For the S stars, a spectroscopic detection of time dilation is expected around pericenter passage (Zucker et al. 2006).

2. *Orbit perturbations* are a test of space curvature, and at higher order, of black hole spin.

   - The leading order precession of orbital periapse is well measured in binary pulsars. (For a discussion of how pulsar timing effects scale to the Galactic-center region, see Pfahl & Loeb 2004, .) Astrometric measurement of precession in the orbit of S2 is considered feasible with current instruments (Eisenhauer et al. 2009), but the long orbital period, and the likelihood of Newtonian precession due to the distributed mass, both present serious difficulties. If stars much further in are discovered, however, precession of orbital planes due to higher-order spin and quadrupole effects become accessible (Will 2008; Merritt et al. 2010).

   - Orbital decay due to gravitational radiation is not considered measurable because of the long time scales and the extreme mass ratio between the star or pulsar and the supermassive black hole.

   - In contrast to the above secular effects, there are also GR induced velocity perturbations, which vary along the orbit (Kannan & Saha 2009; Preto & Saha 2009). In binary pulsars, velocity perturbations are not considered especially interesting and are subsumed within Roemer delays. For Galactic center stars however, the situation is different. First, the velocity perturbations are larger, and second, they are concentrated around pericenter passage, thus offering a better prospect for isolating relativistic from Newtonian perturbations.

3. *Light paths and travel times* are affected by the black hole mass, and again at higher order, by spin.

---

[*]In this paper the semi-major axis a and the pericenter distance $a(1-e)$ are always expressed in units of GM/c^2 and are therefore dimensionless.

- Strong deflection of starlight (Bozza & Mancini 2009) or a pulsar beam (Wang et al. 2009b,a) would be a spectacular though rare event.

- Small perturbations of photon trajectories, too small to measure astrometrically, can nevertheless produce detectable changes in the light travel time. In the pulsar literature this is known as the Shapiro delay. The analogous effect for S stars is a time-dependent redshift contribution (Angélil & Saha 2010), which for a star like S2 is comparable to the velocity perturbations. Hence, in the Galactic center, relativistic perturbations on both orbits and light paths must be considered.

Later in this paper, we will group time dilation with the orbital effects.

Motivated by the above considerations, in this paper we develop a method to fit a relativistic model to observables. This strategy (i) takes relativistic perturbations on both the orbits and the light into account, (ii) treats stellar spectroscopy and pulse timing in a unified way, and (iii) is well suited to analyzing data obtained from a single orbital period or even less. We include the effects of time dilation, space curvature, frame dragging, and torques from the black hole spin. Some further issues remain; most importantly, how to include Newtonian perturbations (from mass other than the black hole's) in the fit — hence the "towards" in the title.

The observable we consider is the apparent frequency ν. As remarked above, this can refer to spectral lines or pulses. The source frequency ν_0 is in principle known for stars, but unknown for pulsars. Note that

$$c \ln(\nu_0/\nu) = c \ln(1+z) \simeq cz \tag{1}$$

where z is redshift in the usual definition. For this paper, however, we will use "redshift" to mean $c \ln(\nu_0/\nu)$. The possibly unknown source frequency now appears as a harmless additive constant in the redshift. For the S stars, the current spectroscopic accuracy is $\approx 10 \, \text{km s}^{-1}$ under optimal conditions (Gillessen et al. 2009a). If a pulsar on a similar orbit is discovered, the accuracy would likely be much higher. Taking, as an example, a one-hour observation with pulses timed to $3 \, \mu\text{s}$ (cf. Janssen et al. 2010) implies an accuracy of one part in 10^9, equivalent to a redshift accuracy of $30 \, \text{cm s}^{-1}$. The same level of accuracy is not inconceivable from spectroscopy of S stars, since planet searches routinely achieve $\Delta v < 1 \, \text{m s}^{-1}$ (e.g. Lovis et al. 2006), but would require some technical breakthroughs to achieve for faint infrared sources like the S stars.

For a given orbit and redshift accuracy, the principal quantities we will calculate are the signal-to-noise ratio S/N for different relativistic effects. For each of four relativistic effects — time dilation, space curvature, frame dragging, and torque — we will present the results in two ways: (i) the redshift accuracy needed to reach some S/N for a given orbit, and (ii) the orbital parameters needed to reach some S/N for a given redshift accuracy.

2. Model

The main calculations in this paper will assume that the trajectories of both S stars (or pulsars) and photons are geodesic in a pure Kerr metric. Naturally, geodesics of the former are timelike, and the latter null. Even if Einstein gravity is correct, the pure Kerr metric is naturally an approximation because this solution to the field equations neglects all mass in the vicinity of the black hole (more on this later), and the mass of the star itself. In general relativity, geodesic motion is fully described by the super Hamiltonian

$$H = \tfrac{1}{2} g^{\mu\nu} p_\mu p_\nu, \tag{2}$$

with $H = 0$ for null geodesics.

Rather than carry out all computations with the Hamiltonian resulting from the full Kerr metric, it is useful to consider two different approximations for the cases of orbits and light paths. These we will call H_{star} and H^{null}. (Word labels in subscripts indicate orbits, in superscripts light paths.) We express these approximate Hamiltonians perturbatively as

$$H_{\text{star}} = H_{\text{static}} + \epsilon^2 \, H_{\text{Kep}} + \epsilon^4 \, H_{\text{Schw}} + \epsilon^5 \, H_{\text{FD}} + \epsilon^6 \, H_{\text{q}}, \tag{3}$$

and

$$H^{\text{null}} = H^{\text{Mink}} + \epsilon^4 \, H^{\text{Schw}} + \epsilon^6 \left(H^{\text{FD}} + H^{\text{q}} \right), \tag{4}$$

where the meanings of the various component Hamiltonians will be explained shortly. Note that ϵ is just a label to indicate orders: if ϵ^n appears, the term is of order v^n (where v is the stellar velocity in light units), but numerically $\epsilon = 1$. The series in (3) and (4) actually consist of the same terms, but because H_{star} is to be applied only to trajectories that are strongly timelike, and H^{null} only to compute null geodesics, the orders of same terms are often different.

Expressions for all the Hamiltonian terms are derived perturbatively from the Kerr metric, using the basic method explained in Angélil & Saha (2010). We will not repeat the details here, but simply list the terms and their physical meanings.

First we consider the orbit (Equation 3).

- To leading order, the star feels no gravity and the clock simply ticks:

$$H_{\text{static}} = -\frac{p_t^2}{2}. \tag{5}$$

- At next-to-leading order, gravity first appears, with

$$H_{\text{Kep}} = \frac{p_r^2}{2} + \frac{p_\theta^2}{2r^2} + \frac{p_\phi^2}{2r^2 \sin^2 \theta} - \frac{p_t^2}{r}, \tag{6}$$

  which is the classical Hamiltonian modified by $1/r \to p_t^2/r$. This modification leaves the problem spatially unchanged, but introduces a temporal stretching causing a gravitational time dilation. This is originally a consequence of the Einstein Equivalence Principle, and affects the redshift at $\emptyset(v^2)$.

- Appearing next are the leading order Schwarzschild contributions,

$$H_{\text{Schw}} = -\frac{2p_t^2}{r^2} - \frac{p_r^2}{r}, \tag{7}$$

  of which the first term effects a further time dilation, and the second curves space, leading to orbital precession.

- Next, the first spin term emerges with

$$H_{\text{FD}} = -\frac{2sp_t p_\phi}{r^3}. \tag{8}$$

  producing frame dragging, an r-dependent precession around the spin axis. Here s is the spin parameter, which points in the $\theta = 0$ or $+z$ direction. Maximal spin is $s = 1$.

- The last set of orbital terms we will consider are

$$H_{\mathrm{q}} = s^2 \left(\frac{\sin^2 \theta p_r^2}{2r^2} - \frac{p_\phi^2}{2r^4 \sin^2 \theta} + \frac{\cos^2 \theta p_t^2}{r^3} - \frac{\cos^2 \theta p_\theta^2}{2r^4} \right), \tag{9}$$

  which are the leading-order quadrupole moment terms. These result in the orbit being torqued towards the spin-plane, as well as other less intuitive effects.

Then we consider light paths (Equation 4).

- At leading order, we have

$$H^{\mathrm{Mink}} = -\frac{p_t^2}{2} + \frac{p_r^2}{2} + \frac{p_\theta^2}{2r^2} + \frac{p_\phi^2}{2r^2 \sin^2 \theta}, \tag{10}$$

  which is to say, the spacetime is Minkowski and the photon trajectories are straight lines.

- The leading order Schwarzschild contribution

$$H^{\mathrm{Schw}} = -\frac{p_t^2}{r} - \frac{p_r^2}{r} \tag{11}$$

  (which notice is not identical to H_{Schw}) introduces lensing and time delays.

- The frame-dragging term for photons

$$H^{\mathrm{FD}} = -\frac{2s p_t p_\phi}{r^3} \tag{12}$$

  debuts at one higher order than H_{FD}. Frame dragging lenses photons around the black hole in a twisted fashion. A ϕ-dependent time-dilation also occurs.

- Finally, we consider higher order Schwarzschild terms, and quadrupole moment terms

$$H^{\mathrm{q}} = -\frac{2p_t^2}{r^2} + \frac{s^2 \sin^2 \theta p_r^2}{2r^2} - \frac{s^2 \cos^2 \theta p_\theta^2}{2r^4} - \frac{s^2 p_\phi^2}{2r^4 \sin^2 \theta} \tag{13}$$

  which, as before, produce a torque towards the spin plane and as well as some more subtle effects.

The well-known separability properties of the Kerr metric (cf. Chandrasekhar 1983) provide solutions up to quadratures, but not explicit solutions. Analytic solutions for geodesics and null geodesics are available for various special cases, for example for the leading-order Schwarzschild case (D'Orazio & Saha 2010). But the present work uses numerical integration of Hamilton's equations.

3. Calculating redshifts

Given a set of orbital parameters for the star, we calculate a redshift curve, meaning $\ln (\nu_0/\nu)$ against observer time or pulse arrival time, by the following method.

First the orbit is calculated by numerically solving Hamilton's equations for H_{star} (Equation 3). If desired, particular orbital relativistic effects can be isolated by omitting other relativistic terms from H_{star}. The independent variable is, of course, not

time but the affine parameter (say λ). Along this orbit, from pairs of points separated by $\Delta\lambda$, photons are sent to the observer. The difference in proper time between the emission of two photons is

$$\Delta\tau = \frac{\Delta\lambda}{\sqrt{-2\,H_{\mathrm{star}}}}. \tag{14}$$

The photons themselves travel along paths determined by H^{null} (Equation 4) with the additional condition $H^{\mathrm{null}} = 0$. Again, one is free to isolate particular relativistic effects on the photons by discarding terms from H^{null}. If Δt is the difference in the photons' times of arrival at the observer, then

$$\frac{\nu_0}{\nu} = \frac{\Delta t}{\Delta\tau}. \tag{15}$$

This calculation is carried out along the orbital path. Some snapshots of this procedure are illustrated in Figure 2.

Now, photons are emitted from the star in all directions, but we need to find exactly those photons which reach the observer. Solving this boundary value problem is the computationally intensive part. Our algorithm for doing so is explained in Angélil & Saha (2010). In stronger fields, the redshift curve takes longer to compute than in weaker ones, both because the orbit integration needs smaller stepsizes over more relativistic regions, and because the boundary value problem requires more iterations before satisfactory convergence is reached.

The observable redshift is of course a combination of all the relativistic effects atop the classical redshift. One can, however, estimate the strengths of each effect in isolation, by toggling each term in Equations (3) and (4) on and off, and then taking the difference in redshift. Figures 3 and 4 show relativistic redshift contributions measured in this way. These orbits refer to the pericenters of a range of orbits, varying in a but with e and the other orbital parameters fixed at the values of S2. These effects have simple scalings with the orbital period, readily deduced from the scaling properties of the Hamiltonians, and summarized in Table 1. Numerical results in Angélil & Saha (2010) verify that such scalings apply not only at pericenter but all along the orbit.

The extended mass distribution in the Galactic center region, due to all the other stars, stellar remnants and dark matter particles that are present, introduces Newtonian perturbations. The distribution and normalization of this mass are poorly constrained on the scales of interest (Schödel et al. 2009), although some upper limits exist (Gillessen et al. 2009b) and some numerical experiments have been done (Merritt et al. 2010). Assuming spherical symmetry for this distributed mass, models of the form

$$\rho(r) \propto r^{-\gamma} \tag{16}$$

are sometimes adopted. Such a model ignores the torques due a nonspherical or discrete mass distribution, and the only change it implies in the orbital dynamics is an additional (prograde) pericenter advance. Figure 5 compares the orbital and photon signals strengths for each effect, including an extended mass distribution of the type (16). Note however, that in the analysis which follows, we do not attempt to include the effects of the extended mass distribution.

4. Fitting

The computational demands for the present work are far greater than calculations of a few redshift curves for given parameters (as in Angélil & Saha 2010), because *fitting* redshift curves in a multidimensional parameter space requires evaluations of up to tens of thousands of such curves. To this end, parallel functionality was added to the implementation. The work is

distributed evenly among the available processors. A workload is the charge of calculating the redshift from a single position on the star's orbit, i.e., a single evaluation of (15), calling for the finding of two photons travelling from star to observer. The program is available as an online supplement.

4.1. The parameters

The redshift curve of an S star or pulsar depends on eight essential parameters, but there can be any number of additional parameters for secondary effects. In this paper we consider nine parameters in all, as follows.

- The black hole mass $M_{\rm BH}$ sets the overall time scale, and accordingly we express it as a time. Changing $M_{\rm BH}$ simply stretches or shrinks the redshift curve in the horizontal direction.

- The intrinsic frequency ν_0 for pulsars is the pulse frequency in proper time, whereas for spectroscopy, it has the interpretation of absolute calibration. Altering ν_0 simply shifts the redshift curve vertically.

- Then there are the Keplerian elements, referring to the instantaneous pure Keplerian orbit with the initial coordinates and momenta. Our orbit integrations all start at apocenter.

  1. The semi-major axis a (or equivalently the period $P = 2\pi a^{3/2} M_{\rm BH}$) is single most important parameter dictating the strength of the relativistic signals.

  2. The eccentricity e sets how strongly peaked the redshift curve is at pericenter.

  3. The argument of pericenter ω sets the level of asymmetry of the redshift curve.

  4. The orbital inclination I changes the amplitude of the redshift. Classically, the inclination enter the redshift depends only on $M_{\rm BH} \sin^3 I$ (on $M_{\rm BH}^3/M_{\rm total}^2 \sin^3 I$ for finite mass ratio). In relativity, the degeneracy is broken, because time dilation is independent of I.

  5. The epoch ϵ_0 basically the zero of the observer's clock.

  The longitude of the ascending node Ω does not appear, because, in our chosen coordinate system, Ω rotates the whole system about the line of sight, which has no effect on the redshift. Formally, we simply fix $\Omega = 0$.

- For the pulsar case, we include a simple spin-down model, with a constant spin-down rate $\nu_0 \to \nu_0 - \dot{\nu}(t_a)$. Here $\dot{\nu}$ is an additional parameter.

We take the black hole spin as maximal, and to point perpendicular to the line of sight. Proper motion of the black hole is not considered.

To fit, we use a quasi-Newton limited-memory Broyden-Fletcher-Goldfarb-Shanno optimization routine with bounds (Zhu et al. 1994; Byrd et al. 1994).

4.2. Signal to noise

With an orbit fitting algorithm in hand, we now need to quantify the notion of detectability of particular relativistic effects. One way would be to attach a coefficient to each term in the relativistic Hamiltonians and then see how accurately that coefficient can be recovered. For this paper, however, we take a simpler approach. Since, for now, we only aim to identify which effects and which regimes are promising, we will simply attempt to estimate the threshold for detecting the presence of each term in the Hamiltonians (3) and (4). Accordingly, we proceed as follows.

1. For some chosen parameters, we generate a redshift curve including all Hamiltonian terms up to some $\emptyset(\epsilon^n)$. These redshift curves are sampled at 200 points, with dense sampling near pericenter.

2. We add Gaussian noise to the redshifts, at some chosen level.

3. We then fit the parameters, with a redshift curve *lacking* a particular Hamiltonian contribution. If the noise level is too high, a reduced $\chi^2 \simeq 1$ will be obtained, otherwise χ^2_{red} will be higher. We define

$$S/N \equiv \sqrt{\chi^2_{\mathrm{red}}} \tag{17}$$

as the signal to noise.

Naturally, it is necessary to check that a large χ^2_{red} is not the result of some algorithmic problem, by verifying that a good fit is obtained if the Hamiltonian term in question is consistently included.

4.3. Redshift-accuracy demands for S2

Figure 6 shows the S/N of time dilation, space curvature, frame dragging, and quadrupole terms, all as a function of redshift accuracy, assuming the orbit of S2. Time dilation is well above the current spectroscopic threshold of $\approx 10\,\mathrm{km\,s^{-1}}$. Space curvature is somewhat below, while frame dragging and quadrupole are far below.

The detectability thresholds are summarized in the first part of Table 2.

4.4. Orbit-size demands for given redshift accuracy

In Figures 7, 8 and 9, the redshift accuracy is set to $10\,\mathrm{km\,s^{-1}}$, $1\,\mathrm{km\,s^{-1}}$ and $30\,\mathrm{cm\,s^{-1}}$ respectively, while the orbital period varies along the horizontal axis.

Table 2 summarizes the detectability thresholds.

5. Summary and Outlook

This paper addresses the problem shown schematically in Figure 2, which is to infer orbital parameters and detect relativistic effects from redshifts or pulsar timings along an orbit. The specific observable of interest is the ratio of rest-frame to observed

frequency ν_0/ν and how it varies along an orbit, especially around pericenter. It is not necessary to measure ν_0 separately, it can be treated as a parameter to be inferred. As a result, spectroscopic redshifts and pulsar timings can be treated in a unified way. We argue that redshift variation over one or a few orbits, with special attention given to pericenter passage, is likely to prove the most useful way to test relativity using Galactic-center stars, or (if discovered) pulsars on similar orbits. There are two reasons why a different strategy is called for here than in the binary pulsar case. First, pericenter speeds of S stars are typically much higher than those of binary pulsars, and second, the orbital periods are too long for cumulative effects to build up.

The observable redshift contains several different relativistic contributions affecting the orbit of the star or pulsar and the light traveling to the observer. For calculations, we use a four-dimensional perturbative Hamiltonian formulation derived from the Kerr metric. Each relativistic effect appears conveniently as a Hamiltonian term that can be toggled on and off to examine its import. Computation of redshift curves using this Hamiltonian approach was demonstrated in a previous paper (Angélil & Saha 2010). In this paper we have developed a pipeline for solving the inverse problem of inferring the orbital parameters from a redshift curve. We then compute the redshift resolution needed to distinguish between redshift curves with and without each relativistic perturbation included, thus simulating the analysis of future observations. The redshift resolution needed to uncover each effect is a few times finer than the maximum contribution of that effect.

In our treatment, we have assumed that frequency data is the only observable at hand. The prospects for detection would be improved if astrometric information were included in the fitting procedure. Information provided by astrometry is particularly potent in constraining the angular Keplerian elements, and would alleviate the burden placed on spectroscopy or pulse timing.

A further way in which the detection prospects could be improved would be to obtain data from multiple orbits. The analysis of frequency data from stars or pulsars with periods < 1 yr would not only benefit from the steep period-dependence of the relativistic effects, but would also boost our chances of resolving cumulative effects. Precession effects are naturally of this type.

Figure 6 illustrates the redshift accuracies required for S2. With current instrumentation, capable of $\sim 10 \, \mathrm{km \, s^{-1}}$ accuracies, detecting time dilation appears comfortably feasible. Detecting space curvature appears feasible with a modest improvement in redshift resolution. On the other hand, the discovery of a pulsar on an orbit comparable to S2 could push the effective redshift accuracy to $< 1 \, \mathrm{m \, s^{-1}}$ and, in principle, bring frame dragging and even quadrupole effects within reach, as shown in Figure 9.

This paper, however, assumes a source of negligible mass in pure Kerr spacetime. The finite mass of S2 (being $< 10^{-5} M_{\mathrm{BH}}$) would perturb the redshift by a similar factor, via its effect on the motion of the supermassive black hole. This would be much smaller than the space-curvature effect, but more than the frame-dragging contribution. A potentially much more serious problem, however, is the Newtonian perturbations due to other mass in the Galactic centre region. This Newtonian "foreground" is not necessarily fatal – the very specific time-dependence of the relativistic effects may enable them to be extracted from under a larger Newtonian perturbation (Merritt et al. 2010) – but further research is needed to assess this.

If sources inwards of S2 are discovered — something we may hope for from the E-ELT and the Square Kilometre Array (SKA) — the prospects for relativity improve. Pfahl & Loeb (2004) argue that there may be 100 pulsars with orbital periods less than 10 years, although the number may be much smaller (e.g. Merritt 2009). A large fraction of these are expected to be found by the SKA. Not only do the relativistic effects get stronger as we move closer to the black hole, but the Newtonian perturbations are likely to weaken. Figures 7 and 8 shows the orbital periods at which one would need to find stars or pulsars given redshift accuracies of $10 \, \mathrm{km \, s^{-1}}$ and $1 \, \mathrm{km \, s^{-1}}$ respectively. If stars with a period of less than one year are discovered, the prospects become very exciting indeed.

Acknowlegements

REFERENCES

Angélil, R. & Saha, P. 2010, ApJ, 711, 157

Ashby, N. 2003, Living Reviews in Relativity, 6, 1

Bozza, V. & Mancini, L. 2009, ApJ, 696, 701

Byrd, R. H., Byrd, R. H., Lu, P., Lu, P., Nocedal, J., Nocedal, J., Zhu, C., & Zhu, C. 1994, SIAM Journal on Scientific Computing, 16, 1190

Chandrasekhar, S. 1983, The mathematical theory of black holes (Oxford/New York, Clarendon Press/Oxford University Press (International Series of Monographs on Physics. Volume 69), 1983, 663 p.)

D'Orazio, D. J. & Saha, P. 2010, ArXiv 1003.5659

Eisenhauer, F., Perrin, G., Brandner, W., Straubmeier, C., Böhm, A., Baumeister, H., Cassaing, F., Clénet, Y., Dodds-Eden, K., Eckart, A., Gendron, E., Genzel, R., Gillessen, S., Gräter, A., Gueriau, C., Hamaus, N., Haubois, X., Haug, M., Henning, T., Hippler, S., Hofmann, R., Hormuth, F., Houairi, K., Kellner, S., Kervella, P., Klein, R., Kolmeder, J., Laun, W., Léna, P., Lenzen, R., Marteaud, M., Naranjo, V., Neumann, U., Paumard, T., Rabien, S., Ramos, J. R., Reess, J. M., Rohloff, R., Rouan, D., Rousset, G., Ruyet, B., Sevin, A., Thiel, M., Ziegleder, J., & Ziegler, D. 2009, in Science with the VLT in the ELT Era, ed. A. Moorwood, 361–+

Ghez, A. M., Salim, S., Weinberg, N. N., Lu, J. R., Do, T., Dunn, J. K., Matthews, K., Morris, M. R., Yelda, S., Becklin, E. E., Kremenek, T., Milosavljevic, M., & Naiman, J. 2008, ApJ, 689, 1044

Gillessen, S., Eisenhauer, F., Bartko, H., Dodds-Eden, K., Fritz, T. K., Pfuhl, O., Ott, T., & Genzel, R. 2010, ArXiv e-prints

Gillessen, S., Eisenhauer, F., Fritz, T. K., Bartko, H., Dodds-Eden, K., Pfuhl, O., Ott, T., & Genzel, R. 2009b, ApJ, 707, L114

Gillessen, S., Eisenhauer, F., Trippe, S., Alexander, T., Genzel, R., Martins, F., , & Ott, T. 2009a, The Astrophysical Journal, 692, 1075

Janssen, G. H., Stappers, B. W., Bassa, C. G., Cognard, I., Kramer, M., & Theureau, G. 2010, ArXiv e-prints

Kannan, R. & Saha, P. 2009, ApJ, 690, 1553

Kramer, M. & Wex, N. 2009, Classical and Quantum Gravity, 26, 073001

Lorimer, D. R. 2008, Living Reviews in Relativity, 11, 8

Lovis, C., Pepe, F., Bouchy, F., Lo Curto, G., Mayor, M., Pasquini, L., Queloz, D., Rupprecht, G., Udry, S., & Zucker, S. 2006, in Presented at the Society of Photo-Optical Instrumentation Engineers (SPIE) Conference, Vol. 6269, Society of Photo-Optical Instrumentation Engineers (SPIE) Conference Series

Lyubenova, M. & Kissler-Patig, M. 2009, "An Expanded View of the Universe - Science with the European Extremely Large Telescope" (ESO: Garching)

Macquart, J., Kanekar, N., Frail, D. A., & Ransom, S. M. 2010, ApJ, 715, 939

Merritt, D. 2009, ArXiv 0909.1318

Merritt, D., Alexander, T., Mikkola, S., & Will, C. M. 2010, Phys. Rev. D, 81, 062002

Pfahl, E. & Loeb, A. 2004, ApJ, 615, 253

Preto, M. & Saha, P. 2009, ApJ, 703, 1743

Schödel, R., Merritt, D., & Eckart, A. 2009, A&A, 502, 91

Taylor, Jr., J. H. 1994, Reviews of Modern Physics, 66, 711

Wang, Y., Creighton, T., Price, R. H., & Jenet, F. A. 2009a, ApJ, 705, 1252

Wang, Y., Jenet, F. A., Creighton, T., & Price, R. H. 2009b, ApJ, 697, 237

Will, C. M. 2008, ApJ, 674, L25

Zhu, C., Byrd, R. H., Lu, P., & Nocedal, J. 1994

Zucker, S., Alexander, T., Gillessen, S., Eisenhauer, F., & Genzel, R. 2006, The Astrophysical Journal Letters, 639, L21

Effect	Orbit	Light path
Classical	$P^{-1/3}$	
Time dilation	$P^{-2/3}$	
Schwarzschild	P^{-1}	P^{-1}
Frame-dragging	$P^{-3/4}$	$P^{-5/3}$
Quadrupole	$P^{-5/3}$	$P^{-5/3}$

Table 1: Relativistic effects considered in this paper, and how they scale with the orbital period.

Effect	Required redshift accuracy for S2	Required orbital period (yr) for given redshift accuracy		
		$10\,\mathrm{km\,s^{-1}}$	$1\,\mathrm{km\,s^{-1}}$	$30\,\mathrm{cm\,s^{-1}}$
Time dilation	$\sim 60\,\mathrm{km\,s^{-1}}$	~ 50	$\gg P_{S2}$	$\gg P_{S2}$
Schwarzschild	$\sim 3\,\mathrm{km\,s^{-1}}$	~ 13	~ 30	$\gg P_{S2}$
Frame dragging	$\sim 10\,\mathrm{m\,s^{-1}}$	~ 0.5	~ 0.8	$> P_{S2}$
Torque	$\sim 50\,\mathrm{cm\,s^{-1}}$	~ 0.04	~ 0.1	$\sim P_{S2}$

Table 2: Summary of the observational thresholds at which different relativistic effects are exposed, assuming a source of negligible mass in a pure Kerr spacetime.
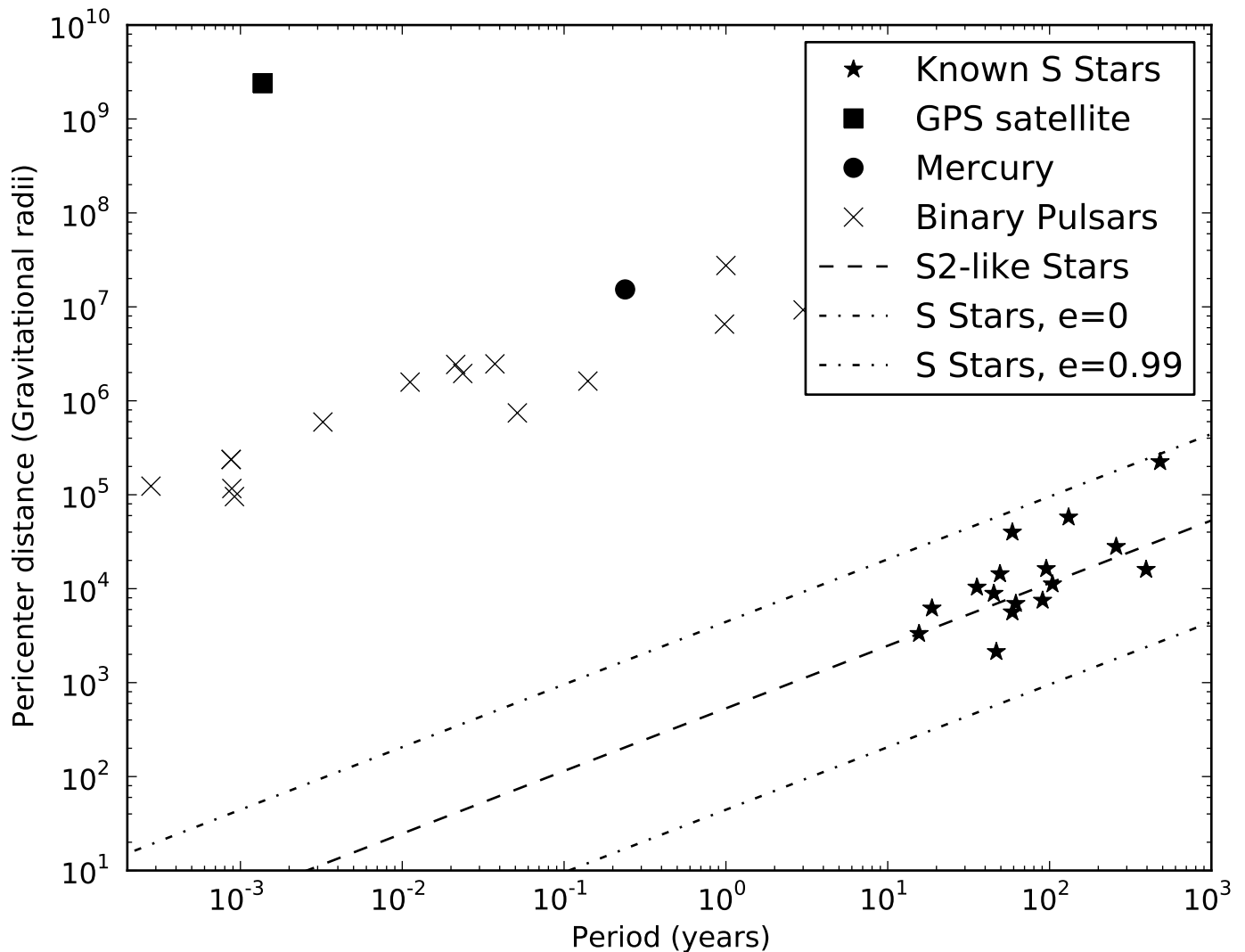
Fig. 1.— Pericenter distance (in units of GM/c^2) against orbital period for a variety of systems. The known S stars, having smaller pericenter distances, are more relativistic than known binary pulsars. But the long orbital periods of the S stars render it infeasible to measure cumulative effects over many orbits. Hence other techniques must be devised. The pulsar examples are taken from Lorimer (2008). For the S stars, the orbital elements in Gillessen et al. (2009a) have been used. In this paper we also treat fictitious stars that lie along the dashed line, that is, having a range of semi-major axis a values but with the same eccentricity and angular elements as S2.
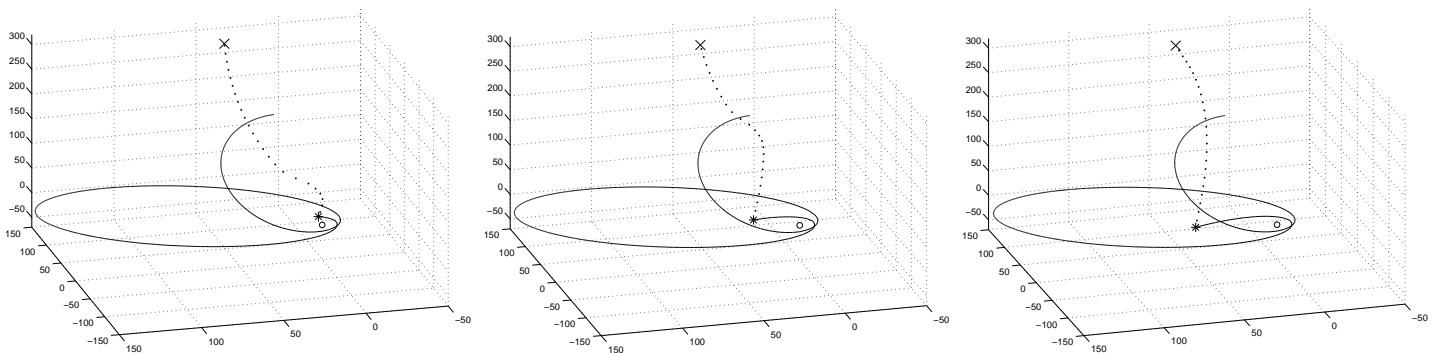
Fig. 2.— A schematic example of the system we deal with - a star on an orbit around the supermassive hole. So as to make the relativistic effects visually discernible, this star has a very low value of $a = 100$ - yet may still lie within the regime that the E-ELT will be able to probe (Lyubenova & Kissler-Patig 2009). The stellar orbit is traced from apocenter, and shown through its second pericenter passage, at three slices of coordinate time. The star emits photons in all directions at equal intervals of proper time, but only the photons which will reach the observer are shown. For sensible calculations, the observer is located much further away and in the direction of the Earth. The photon arrival times give the observed frequency. Both the star and the photons travel on geodesics in a curved spacetime, and as a result, the star's orbit precesses, and the photons are lensed.
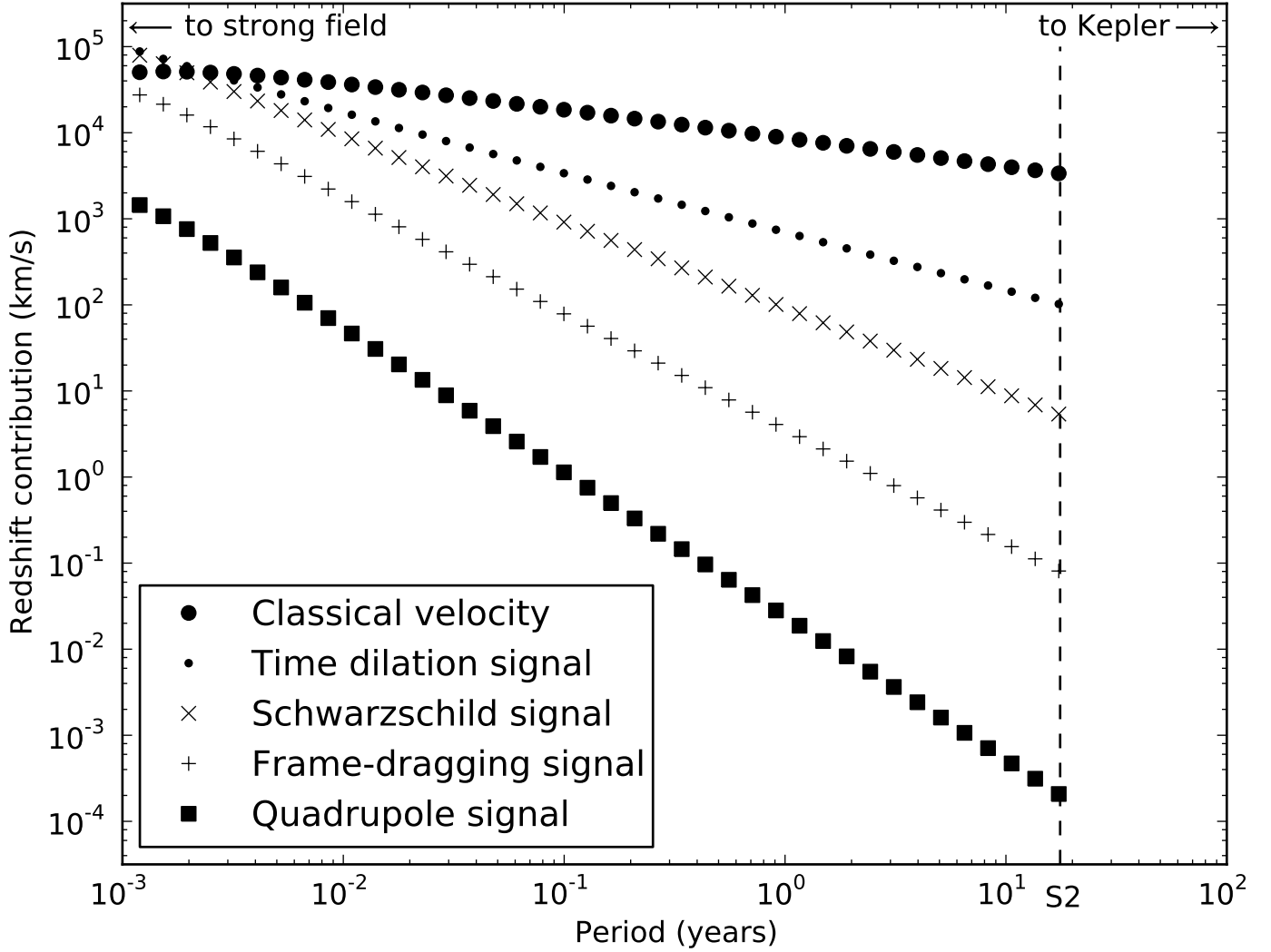
Fig. 3.— Redshift contributions of different orbital effects. Shown here is the contribution of each term in Equation (3) at pericenter, with the orbital period being varied and the other orbital parameters fixed at the S2 values. The pericenter distance varies from 3600 (approximately the value for S2) down to 6. Note that for the last two signals - the frame-dragging and the quadropole - we have taken the black hole spin to be maximal and to point perpendicular to the line of sight. The signal scalings are listed in Table 1. The curves begin to intersect as we move towards the strong field regime - attributable to the the breakdown in our perturbative approximation for small r.
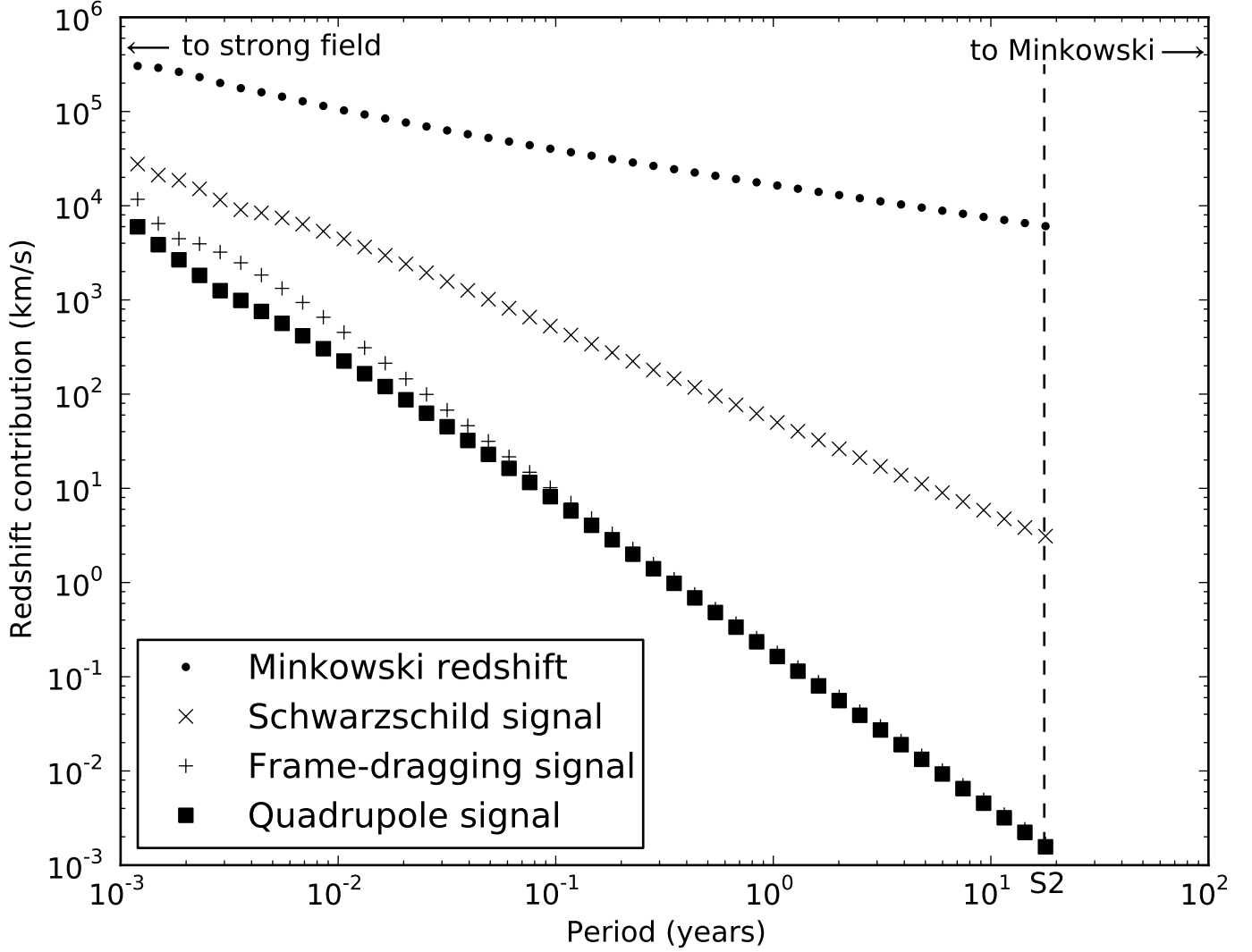
Fig. 4.— Like Figure 3 but for photon propagation delays (Equation 4). The Schwarzschild propagation signal is for the most part slightly smaller than the Schwarzschild orbital signal, and scales in the same way. The frame-dragging propagation signal is considerably smaller than the corresponding orbital signal, and scales like $z^{\mathrm{FD}} \propto P^{-5/3}$, as opposed to $z_{\mathrm{FD}} \propto P^{-4/3}$. The frame-dragging signal remains approximately an order of magnitude weaker on the photons than on the star. This suggests that in attempting to measure the spin of the black hole in the post-Newtonian regime, its manifestation on the orbit is what matters. Note however, that this is not the case for the Schwarzschild effects - for which neither the photon nor orbit perturbations may be neglected.
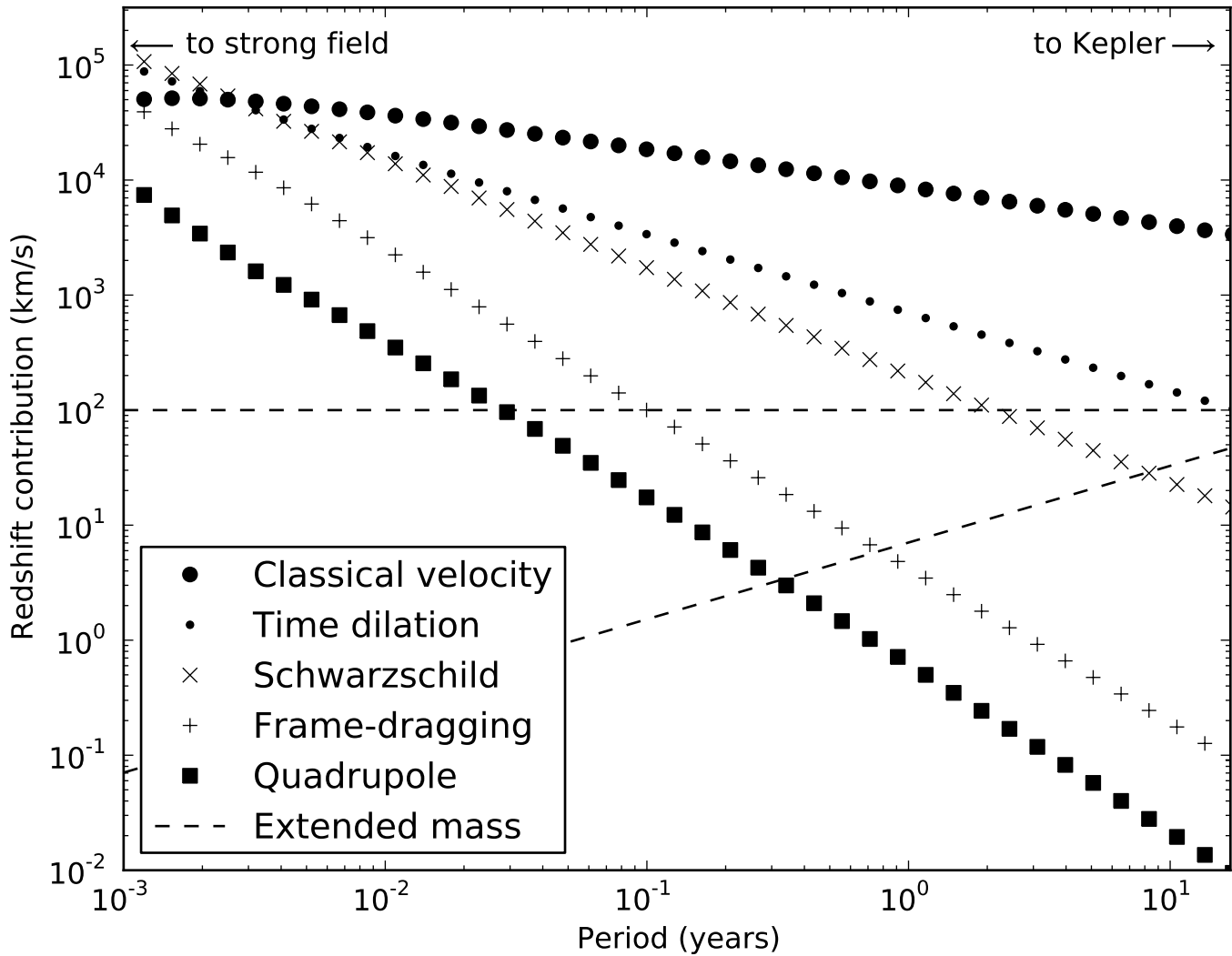
Fig. 5.— Relativistic redshift effects, with orbital and light-path contributions summed. Two estimates for the signal due to the extended mass distribution are also shown, using the crude model (16) normalized so that the circular velocity at the $r = 10^5 \, GM_{\mathrm{BH}}/c^2$ (or $\sim 0.1 \, \mathrm{pc}$) is $\sim 100 \, \mathrm{km \, s^{-1}}$ (cf. Gillessen et al. 2009a). The flat and sloping dashed curves correspond to $\gamma = 2.5$ and 1.5 respectively.
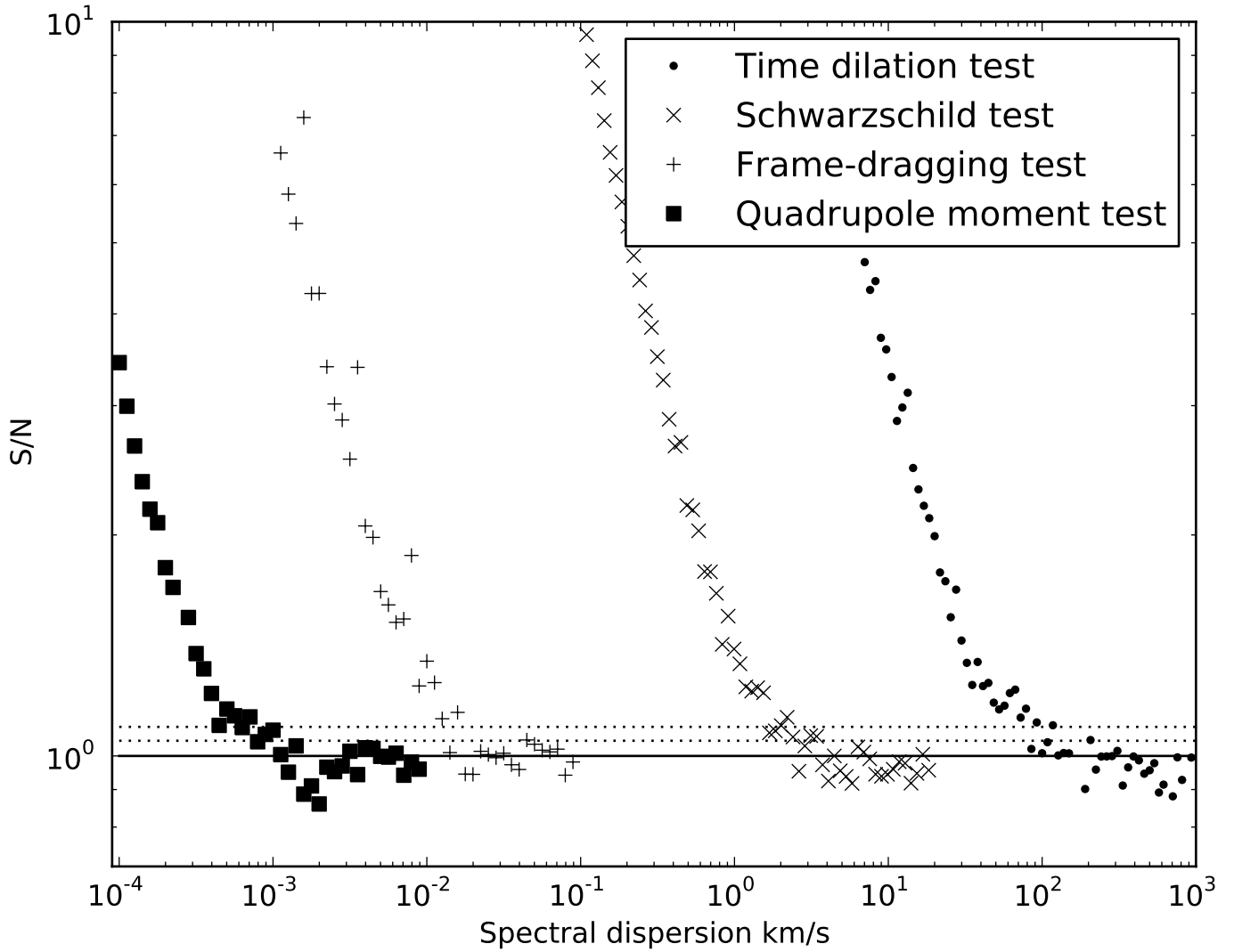
Fig. 6.— The signal-to-noise ratio (as defined by equation 17) for different relativistic effects in the orbit of S2 as a function of redshift accuracy. Each point on this figure corresponds to a simulated data set of 200 redshifts, distributed over the orbit but with highest density around pericenter.
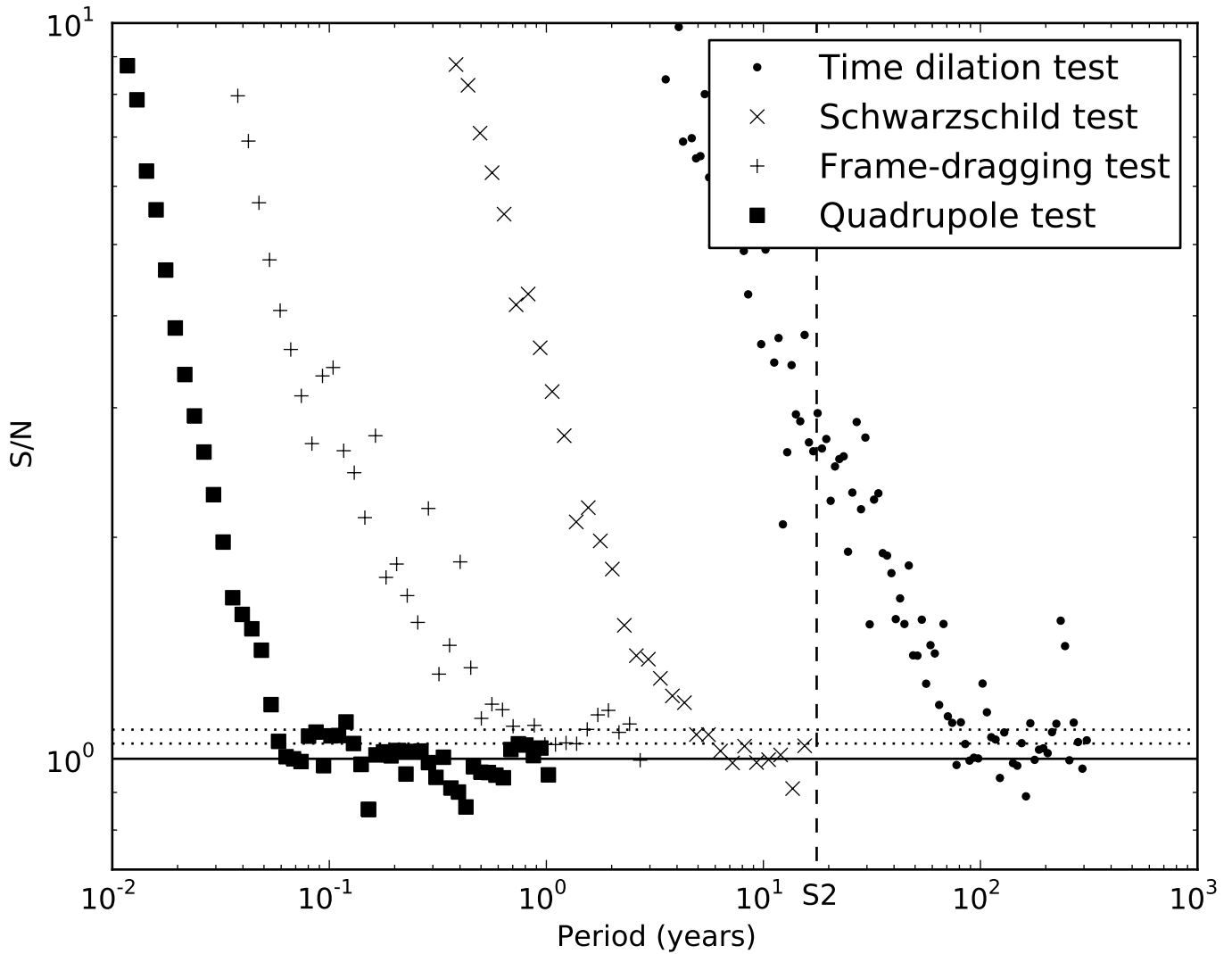
Fig. 7.— Similar to Figure 6, except that the redshift accuracy is fixed at $10\,\mathrm{km\,s^{-1}}$ and the orbits vary, being scaled-down and speeded-up versions of the orbit S2. For large S/N these curves scale with the powers in Table 1. Current instrumentation, operating under optimum conditions, should manage an accuracy of $10\,\mathrm{km\,s^{-1}}$ indicating that gravitational time dilation should be able to be detected on some of the currently known S Stars.
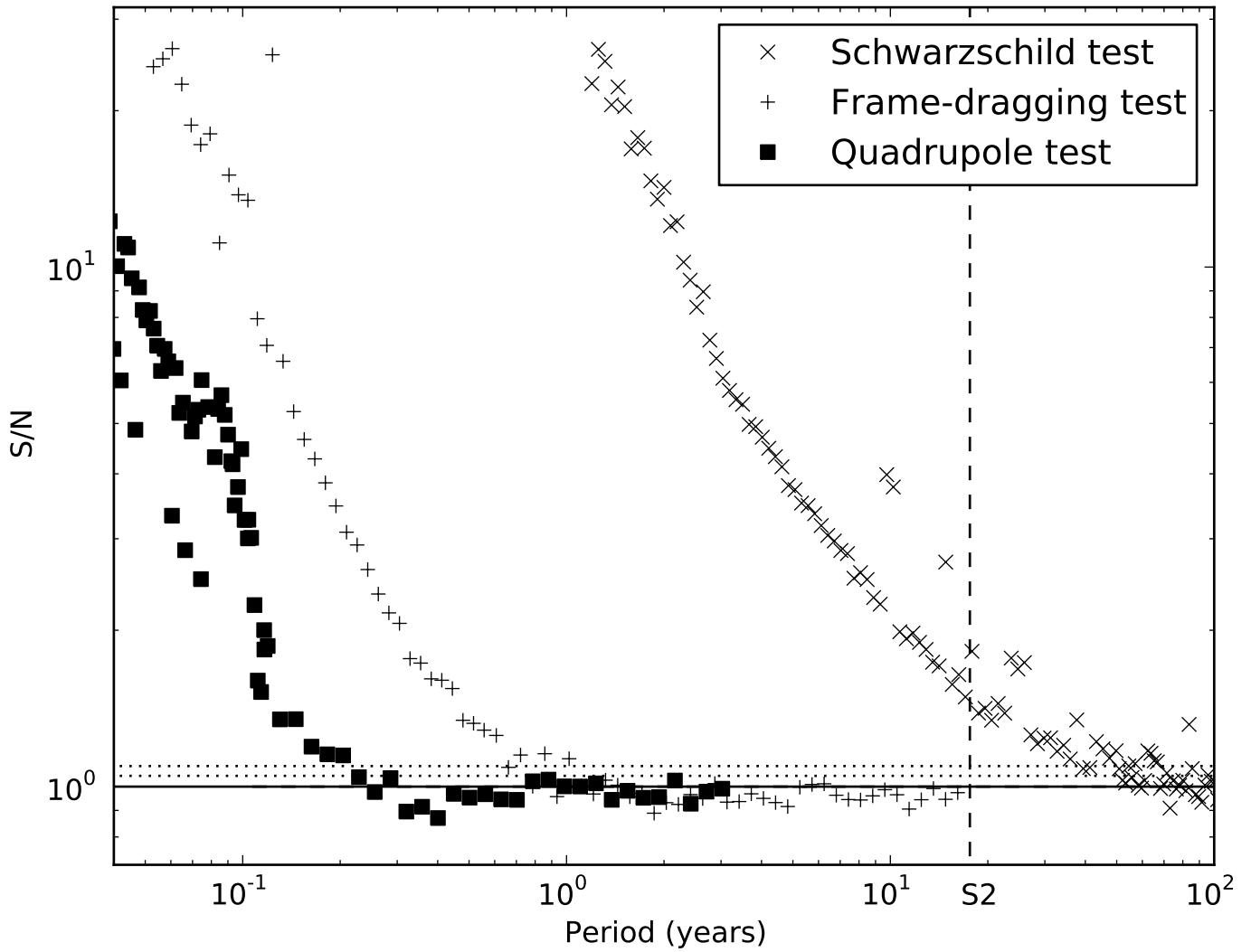
Fig. 8.— Like Figure 7 but for a redshift accuracy of $1\,\mathrm{km}\ \mathrm{s}^{-1}$ - matching the capabilities of the E-ELT (Lyubenova & Kissler-Patig 2009).
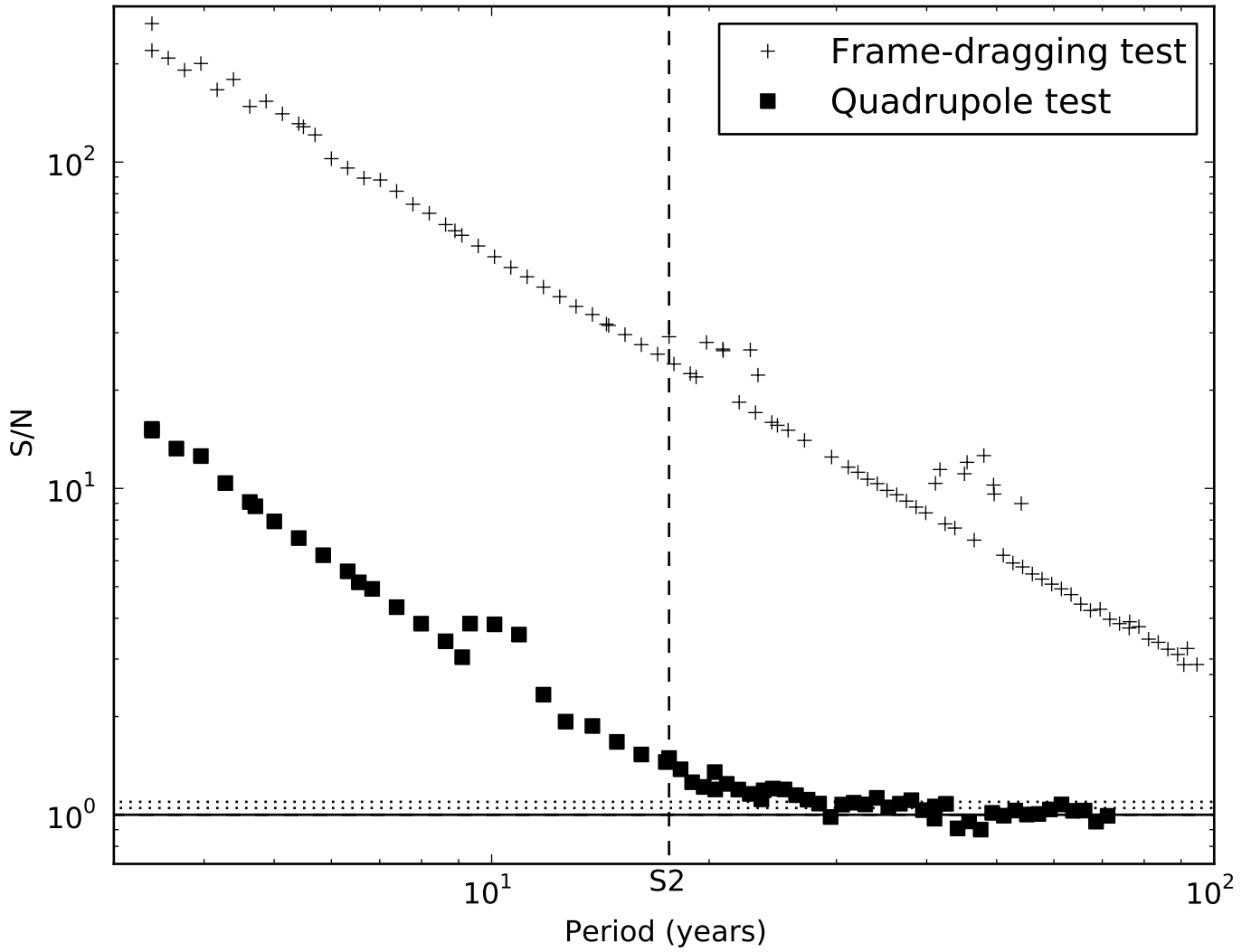
Fig. 9.— Like Figures 7 and 8 but for redshift accuracy $30\,\mathrm{cm\,s^{-1}}$. Pulse timing accuracies at this level are already available, known pulsars orbiting the black hole on suitably short orbits however are not.